Materials Science for Energy Technologies 7 (2024) 205–215

Contents lists available at ScienceDirect

Materials Science for Energy Technologies

journal homepage: www.keaipublishing.com/en/journals/materials-science-for-energy-technologies

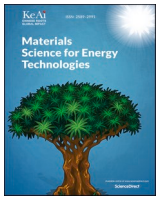

Non-covalent functionalization of surfactant-assisted graphene oxide with silver nanocomposites for highly efficient photocatalysis and anti-biofilm applications

Usan Pathinathan Saleth Prabhakar [a,*], Paramasivam Shanmugam [b], Supakorn Boonyuen [b,*], Lakshmi Prabha Chandrasekar [c], Ramyakrishna Pothu [d], Rajender Boddula [e,*], Ahmed Bahgat Radwan [e], Noora Al-Qahtani [e,f,*]

[a] Department of Chemistry, St. Joseph University, Dimapur 797115, Nagaland, India
[b] Department of Chemistry, Faculty of Science and Technology, Thammasat University, Pathum Thani 12120, Thailand
[c] Department of Chemistry, College of Engineering and Technology, SRM Institute of Science and Technology, Chennai 603 203, India
[d] School of Physics and Electronics, College of Chemistry and Chemical Engineering, Hunan University, Changsha 410082, China
[e] Center for Advanced Materials (CAM), Qatar University, Doha 2713, Qatar
[f] Central Laboratories Unit (CLU), Qatar University, Doha 2713, Qatar

ARTICLE INFO

Keywords:
Surfactant-assisted reduced graphene oxide
Non-covalent functionalization
Silver nanocomposites
Anti-biofilm
Photocatalysis

ABSTRACT

This study presents a comprehensive investigation on the synthesis and characterization of surfactant-assisted graphene oxide non-covalent functionalized silver nanocomposites (rGS-AgNPs) for achieving remarkable photocatalytic and anti-biofilm properties. The approach involves using an anionic surfactant (sodium lauryl sulfate (SLS)), silver nitrate ($AgNO_3$), and reduced graphene oxide (rGO) as stabilizing/reducing agents, metal precursors, and supporting materials, respectively. Different composites were prepared by varying the concentration of $AgNO_3$, resulting in rGS-AgNPs composites with concentrations of 0.9×10^{-3} mM, 1.8×10^{-3} mM, and 2.7×10^{-3} mM. Characterization techniques including XRD, FTIR, SEM, and TEM/EDS analysis confirmed the formation of face-centered cubic AgNPs and amorphous rGO structures. The composites exhibited a firm binding of the surfactant and AgNPs on the surface of rGO nanosheets, resulting in efficient anti-biofilm and photocatalytic activity. The size of the supported AgNPs on rGO/SL was found to be 8–10 nm. The rGS-AgNPs composites displayed significantly improved anti-biofilm and photocatalytic performance, attributed to the increased surface area of AgNPs. Moreover, the photocatalytic efficiency of the rGS-AgNPs composites reached 96.48 % within 60 min, outperforming pure AgNPs. The synthetic procedure and practical applications will be utilized for biosensors, food packing technology, biomedical and pharmaceutically valuable reactions.

1. Introduction

Environmental crises caused by the depletion of natural resources, greenhouse gases, and the increasing pollution resulting from urbanization and industrialization are global concerns. The unchecked and untreated discharge processes have serious effects on both the biotic and abiotic components of the environment [1,2]. Various industries, including leather, textile, paints, cosmetics, plastics, and pharmaceutical companies, release common pollutants such as organic dyes, pigments, gasoline, heavy metals, and highly volatile organic hydrocarbons [3,4]. These pollutants have had a significant impact on humans, animals, and marine life. Specifically, organic dyes are causing substantial pollution in the environment [5]. Industries involved in dyeing, such as those related to paper, cotton, silk, and wood, typically generate significant adverse effects on people. Notably, the presence of Methylene blue (MB) dye in wastewater has been found to be particularly toxic due to the thiazine cationic stain groups [6,7]. Therefore, it is crucial to employ effective methods to remove MB dye from wastewater and continue the ongoing challenge of addressing this issue [8]. Various techniques, including filtration, coagulation, irradiation, chemical oxidation,

* Corresponding authors.
E-mail addresses: salethprabhakar93@gmail.com (U.P.S. Prabhakar), chemistrytu@gmail.com (S. Boonyuen), research.raaj@gmail.com (R. Boddula), noora.alqahatani@qu.edu.qa (N. Al-Qahtani).

https://doi.org/10.1016/j.mset.2023.10.005
Received 30 June 2023; Received in revised form 22 October 2023; Accepted 30 October 2023
Available online 3 November 2023

ozonation, ion exchange, osmosis, electrochemical treatment, adsorption, and precipitation, are recommended for the eradication and removal of dyes from water [9–12]. Additionally, biological processes such as microbial degradation and algae decolorization can be utilized. Among these techniques, the use of nanomaterials-based photocatalytic processes has proven to be particularly effective in this field, with carbon-based nanocomposites receiving significant attention for the degradation of organic dyes.

Another significant environmental crisis is the occurrence of poultry diseases caused by numerous pathogens, which compromise animal health and welfare while reducing production efficiencies. This, in turn, leads to decreased profitability and heightened levels of antimicrobial usage [13,14]. The contamination of poultry food products with various zoonotic pathogens also poses concerns for food safety and public health, particularly with the increasing consumer awareness and demand for organic poultry products. Pathogens such as *Salmonellas* and *Campylobacter spp*. have the ability to form biofilms, which further worsen poultry diseases and contribute to antimicrobial resistance [15]. Biofilms are intricate biological structures composed of multiple bacterial cells enveloped by layers of substances produced by them, creating a barrier that impedes the eradication of these organisms Sevaral methods have been developed to control anti-biofilm activity, with carbon-based nanocomposites receiving significant attention due to their effectiveness in both photocatalytic and anti-biofilm functions [16]. Carbon-based nanomaterials have emerged as promising candidates for a wide range of applications in energy, environment, and biomedicine applications [9,17,18]. Biomedical, energy and environmental fields are interesting and challenging tasks in the current scenario [19,20]. Particularly, the development of toxic-free, cost-effective, and efficient materials is of utmost importance in these fields [21,22]. Carbon-supported materials are plays an important role in biomedical and photocatalytic applications[22,23]. Carbon materials, including graphene, reduced graphene oxide, carbon nanotubes, fullerene and activated carbon have been widely explored as scaffolds for the fabricating nanocomposites [24,25]. Daniel et al. reported the endohedral functionalization of SWCNT's to enhance visible light photocatalysis of organic dyes [26]. Among them, graphene and graphene oxides are good candidates to enhance the stability and activity of the nanocomposites [27,28]. However, the leaching of metals from graphene nanocomposites poses a significant challenge in terms of efficiency and recyclability [29]. To address this, functionalization of graphene has been extensively investigated to enhance stability and activity [30–32]. Various types of methods including chemical vapour deposition, mechanical or thermal exfoliation and epitaxial growth are capable of producing economically favourable rGO on a large scale as compared to other methods[33–35]. Further, improve the metal loading and enhance the activity to attach some stabilizing agent viz., polymers, surfactant and enzymes [36,37]. Surfactants have garnered attention as effective agents for the functionalization of graphene, as they strongly attach to graphene, control nanoparticle size, and prevent aggregation. Jing et al investigated the various types of surfactants functionalized rGO for enhance the solubility properties [38]. Normally, two types of methods that have to be used for the functionalized with rGO, the methods such as covalent functionalization and non-covalent functionalization. Non-covalent functionalization methods, rather than covalent methods, are preferred due to their ability to modify the surface without introducing structural changes or defects [30,39]. Vasilos et al. reviews briefly discussed the non-covalent functionalization of graphene and graphene oxide utilized for energy storage devices, catalysts, bio-sensing and biomedical field [40]. To improve the active surface/activity metal nanoparticles have been considered the greater attention [41]. Ag and AuNPs have been greater antibacterial and photocatalytic properties. On comparing Ag and Au, the AgNPs are economically highly active against the anti-biofilm and photocatalytic applications. Yugal et al. reported the Indian medicinal plant's extract stabilized AgNPs utilized as anti-biofilm and antibacterial agent [42]. The surfactant and reduced graphene oxide are used to prevent the agglomeration and oxidation of the photocatalysts, thus aiding in the catalysts' reusability [43,44]. To overcome this problem, a suitable surfactant is coated onto the rGO surface to prevent AgNPs aggregation. Further, The aim of this study was to investigate the preparation of eco-friendly non-covalent functionalized surfactant-coated graphene oxide supported AgNPs. The resulting composites, known as rGS-AgNPs, were utilized for both the photodegradation of methylene blue and anti-biofilm activity. The non-covalent functionalization method helps prevent structural defects on the surface of the rGO. The current synthesis process may face challenges when scaled up for industrial applications. Further research is needed to optimize production methods for larger quantities. In the future, we plan to prepare various types of surfactant-coated materials, including cationic, anionic, and non-ionic surfactants, applied onto graphene oxide and other related carbon materials. These modified materials will find applications in biosensors, food packaging technology, as well as in valuable reactions within the biomedical and pharmaceutical fields.

2. Experimental methods

2.1. Materials

Graphite and silver nitrate ($AgNO_3$) was purchased from Sigma Aldrich chemicals Pvd. Ltd., Mumbai, India. Sodium lauryl sulfate (SLS) was purchased from Loba cheme. Pvt. Ltd.

2.2. Synthesis of rGS-AgNPs

Graphene oxide (GO) was prepared by modified Hummer's method [45]. The reduced graphene oxide was prepared in earlier literature [46]. The rGO/SL was prepared as follows: initially, 100 mg of rGO was dispersed in 50 mL of water for 8 h under ultra-sonication. Add 50 mg of SLS surfactant into the above rGO solution and stirred magnetically for 5 h. Then, 0.9 mM of $AgNO_3$ (15 mg) was added to the above reaction mixture and thus obtained rGSL-Ag^+. The Ag^+ ion was reduced by Ag^0 by the addition of $NaBH_4$ The After addition of $NaBH_4$, the colour of the solution turned colourless into yellow, thus confirming the formation of AgNPs. The rGS-AgNPs were purified and collected through a centrifugation process. The resulting rGS-AgNPs composites were obtained by freeze-drying at −51 °C for 36 h. Furthermore, three different rGS-AgNPs composites were prepared by changing the concentration of Ag^+ ions using a simple synthetic procedure. The composites obtained were named rGS-Ag-1, rGS-Ag-2, and rGS-Ag-3, respectively.

2.3. Photocatalytic activity

The photocatalytic efficiency of the as-prepared rGO, rGO/SL, rGS-Ag-1, rGS-Ag-2 and rGS-Ag-3 were examined through photodegradation of MB under visible light irradiation. Briefly, 5 mg of the photocatalysts were suspended in 40 mL of MB (10 mg/L) solution. The suspension was stirred for 30 min in the dark condition to achieve the adsorption–desorption equilibrium over the catalyst and dye solution. After 30 min, the solution was stimulated with 150 W Xe lamb as a light source. At a particular interval of time, 5 mL of the sample was withdrawn to remove the catalyst particles from the solution using a centrifugal process. The concentration of the MB during the degradation process was monitored using a UV–Visible spectrophotometer. The stability of the photocatalysts was done by recyclability test under similar reaction conditions.

2.4. Bio-film activity

To appraise the potency of the nanocomposites in intruding the biofilm formation using microtiter plate (MTP) assay. The wells were packed with 180 μL brain heart infusion (BHI) broth and inoculated with 10 μL of pathogenic bacterial culture for 24 h. To this 10 μL

nanocomposites were added in various concentrations (500, 250, 125, 62.5, and 31.25 μg/mL) and were incubated at 37 °C for 24 h. Subsequently after incubation, the contents in the wells were removed, and washed with phosphate buffer saline to remove free-unreacted species. The adherence of sessile bacteria was further interpreted by the addition of sodium acetate (2 %) and stained with crystal violet (0.1 % w/v.). Further, dried plates were decanted and optical density was evaluated using a microtiter plate reader (Thermo) at 600 nm. The percentage of biofilm inhibition was calculated using the below formula

$$\%\ \text{Biofilm inhibition} = \frac{(Control\ OD - Test\ OD)}{Control\ OD} \text{ X } 100 \quad (1)$$

3. Results and discussion

The XRD spectra of the as-prepared rGO, rGO/SL, rGS-Ag-1, rGS-Ag-2, and rGS-Ag-3 composites were shown in Fig. 1a. The XRD analysis confirmed the crystallinity and phase purity of the nature of rGO and AgNPs. The XRD pattern of the rGO shows a high index, strong broad peak and small peak at $2\theta = 23.86°$ and 43.01° for (002) and (101) planes, respectively, thus diffraction peaks support the formation of hexagonal graphene structure [47,48]. In rGO/SL composites, similar rGO peaks appeared and both graphene oxide and SL functionalized GO shows an amorphous patten. But the rGO peak intensity is slightly reduced on rGO/SL composites, due to the non-covalent functionalization of surfactant onto rGO surface. Haixin et al reported the similar XRD pattern for the surfactant coated graphene oxiede using non-covalent spin coating method [49]. XRD diffraction pattern of rGO/SL-AgNPs (rGS-Ag) composites, major diffraction peaks appeared at $2\theta = 38.08°$, 44.01°, 64.19° and 74.03°, which corresponded to (111), (200), (220) and (311) planes, respectively. The obtained diffraction peaks are in good agreement with the pure phase-centered cubic structure of AgNPs (JCPDS card no. 96-110-0137) [50,51]. The peak intensities of AgNPs are increased with increasing the metal loading of Ag^+ ions (0.9 mM to 2.7 mM). Further, the average crystalline size was calculated by the - Debye Scherrer equation, $D = K\lambda/\beta Cos\theta$ and an average crystalline size of 8–10 nm was calculated for rGO/SL-Ag-3 based on the most intense (111) peak [9].

Surface functional groups, the interaction between rGO with SL and immobilization of AgNPs onto the rGO/SL surface were characterized by FTIR spectroscopy, as shown in Fig. 1b. FTIR spectrum of rGO, the characteristic peaks appeared at 3432.85 cm^{-1} and 1638 cm^{-1} related to stretching vibrations of –OH and C═O, respectively. Further, the carboxylic moieties and other peaks at 1182.27 cm^{-1}, and 1058.53 cm^{-1} are due to C-H and C-O stretching vibrations (alkoxy groups), respectively. Based on this peak evidence the rGO contains have an abundant number of hydroxyl and oxygen functional groups on the surface [52]. After functionalization of SL onto the surface of rGO, the additional peaks appeared at 1212.31 cm^{-1} and 1045.21 cm^{-1} due to asymmetric and symmetric stretch of the SO_2 functional group, thus evidence confirming the SL surfactant successfully coated onto the surface of rGO. Further, the SL stabilized AgNPs loaded onto the surface of rGO using a simple chemical reduction method. After functionalization with AgNPs in the concentration range of 15 mg to 45 mg, there were observable shifts in the –OH and –C═O peaks. These shifts were attributed to the loading of AgNPs [53]. When comparing the spectra of rGS-Ag-1 and rGS-Ag-2, more significant changes were observed compared to rGS-Ag-3. This suggests that rGS-Ag-3 may have experienced aggregation.

The SEM is one of the most important powerful tools to find out the structural morphological change in prepared composites. The SEM images of the GO, rGO, rGO/SL, rGS-Ag-1, rGS-Ag-2 and rGS-Ag-3 composites were shown in Fig. 2a–f. Fig. 2a shows the SEM images of GO sheets that have smooth surfaces, folded regimes and wrinkle structures [50]. Fig. 2b show the SEM images of rGO showing that slight changes occurred at homogeneous to heterogeneous surface. In Fig. 2c, shows SEM images of rGO/SL, after functionalization of SL with rGO, the heterogeneous block and white layer appeared on the surface of rGO. This evidence predicted that surfactants are tightly packed on the GO surfaces for maximizing the surface charge in the graphitic layers [54]. Yang et al. conducted a study similar SEM images to involving a surfactant-modified graphene oxide complex coating, aiming to functionalize the material for separating water/oil emulsions [55]. In a similar vein, Bárbara et al. reported on various types of surfactants and polymers grafted onto carbon nanotubes using a non-covalent functionalization method. Following the functionalization with surfactants and polymers, the dispersion ability was significantly enhanced, albeit with some occurrence of surface defects [56]. Furthermore, the non-covalent functionalization method does not alter the suffface morphology of the rGO [57]. Further, Fig. 2d–f, shows that the AgNPs are evenly distributed onto the surface of rGO/SL, thus evidence supports the successful loading of AgNPs. Additionally, the intensities of the metal loading increased with increasing the metal ion concentration [50].

Further, the size and surface morphology of the non-covalent functionalized surfactant assisted rGO supported AgNPs composites were studied by HRTEM/EDS and shown in Fig. 3a-g. TEM images reveal a

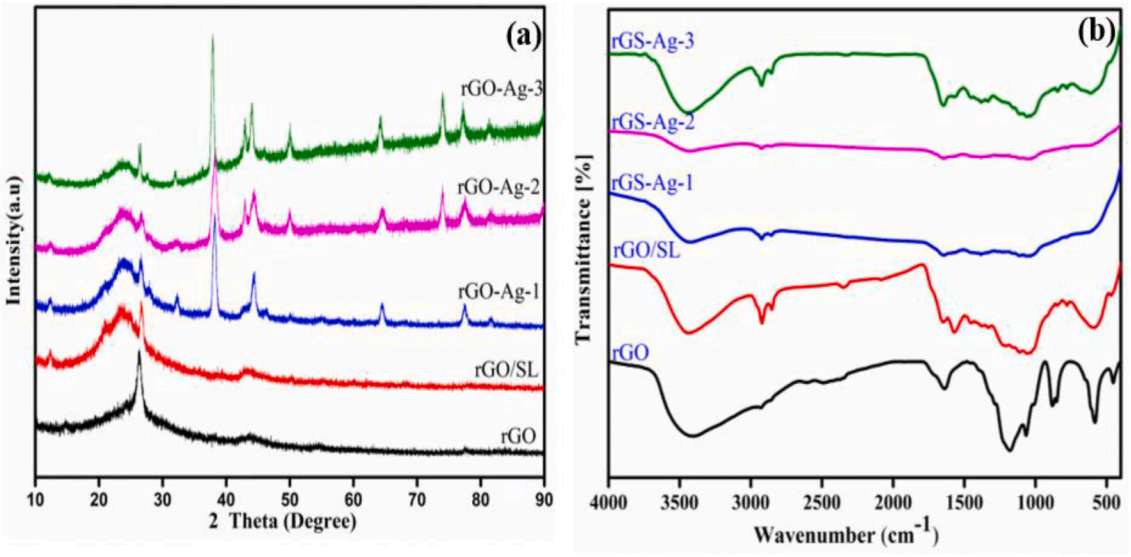

Fig. 1. (a). X-ray diffraction and (b). FTIR spectrum of rGO, rGO/SL, rGS-Ag-1a, rGS-Ag-2, and rGS-Ag-3 composites.

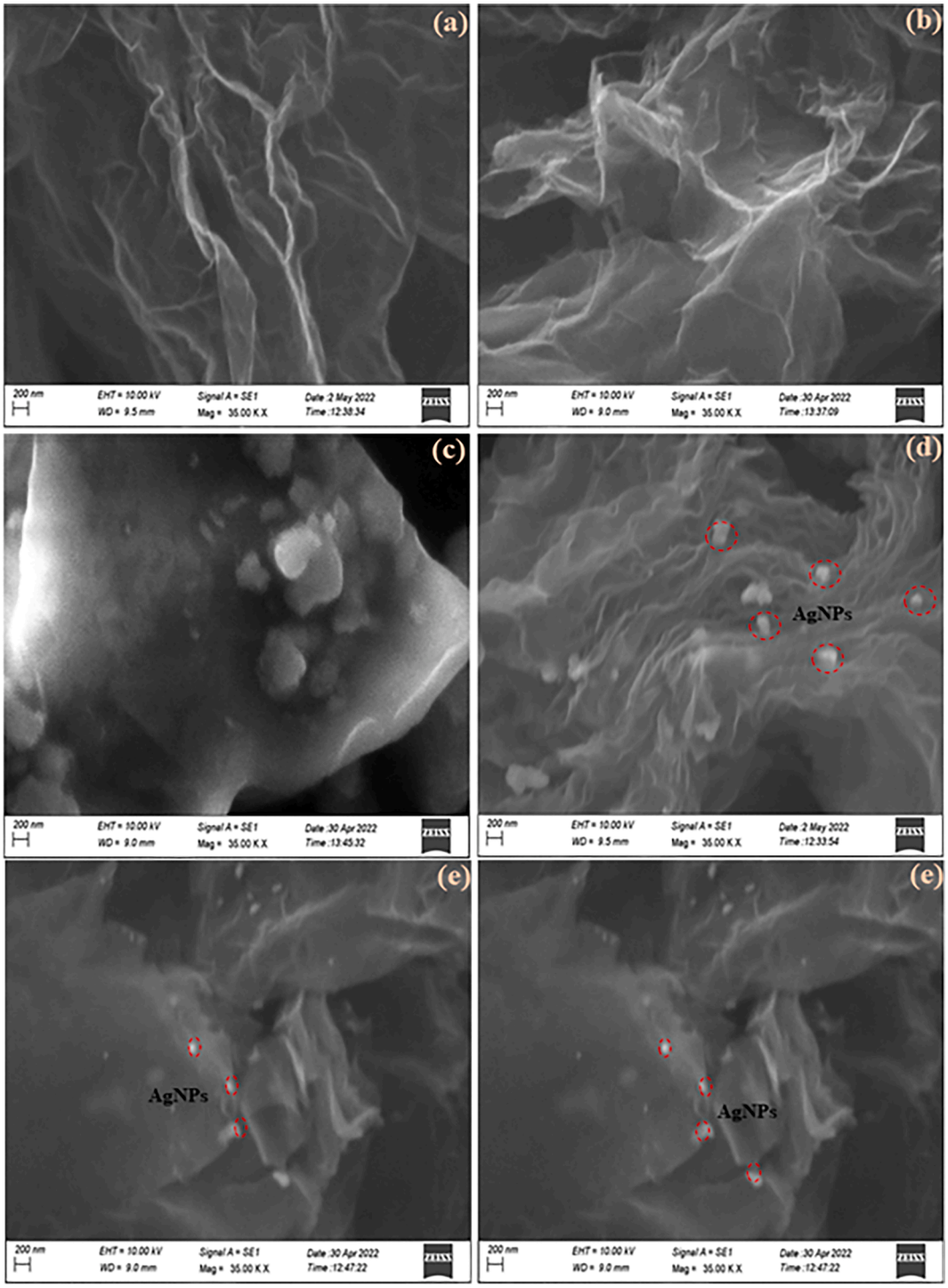

Fig. 2. FESEM images of (a). graphene, (b), rGO, (c). rGO/SL, (d). rGS-Ag-1, (d). rGS-Ag-2 and (e). rGS-Ag-3.

homogenous dispersion, smooth surface and spherical-like AgNPs decorating onto the rGO sheets. Fig. 3a-b showed typical sheet-like waves, and wrinkly and clumped structures with a size of 15–150 nm. Further, spherical AgNPs are uniformly loaded onto the surface of rGO with the size of 8–10 nm [58]. The elemental composition of the prepared rGO/SL-AgNPs composites was analyzed EDS as shown in Fig. 3c. The obtained peaks corresponded to C, O, S and Ag elements, confirming the existence of metallic AgNPs onto the surface of rGO/SL. The presence of O indicates the oxygen-containing groups generated during rGO synthesis. The sulphur (S) elements denote the sulfur-containing surface successfully non-covalent bonded onto the surface of rGO.

3.1. Anti-biofilm activity

In vitro reports of various concentrations of rGO, rGS-Ag-1, rGS-Ag-2, and rGS-Ag-3 reveal the destruction of biofilm formation against the susceptibilities of bacteria *Enterococcus faecalis* -MTCC. No. 439 and the corresponding graph as shown in Fig. 4 and Figs. S1–S4. The minimum inhibitory concentration for rGO, rGS-Ag-1, rGS-Ag-2, and rGS-Ag-3 was inferred at higher concentrations of 500 μg/ml-30.064, 27.61, 44.99, and 31.39 % respectively. The biofilms formed under nutrient-deprived and aerobic environment depicts clearly with obvious signs of surface degradation of dentine. Robert Lotha et al reported the similar types of

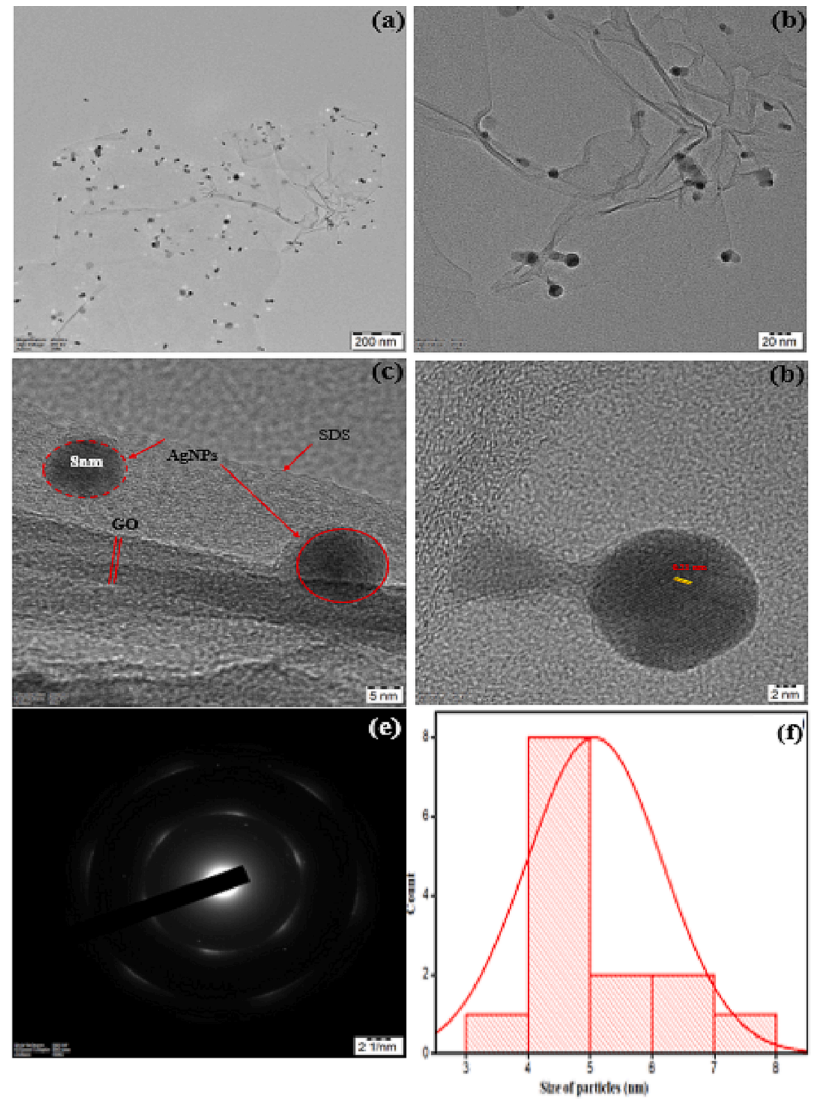

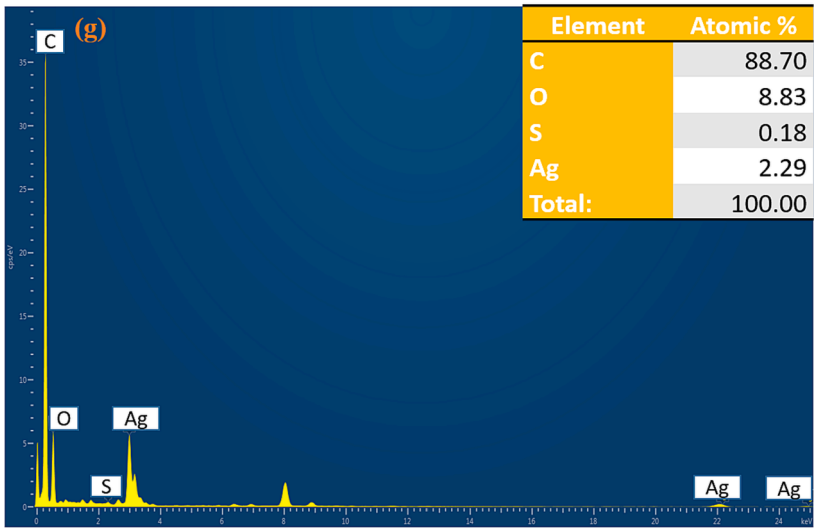

Fig. 3. (a-d) HRTEM images (e). selected area diffraction pattern (SAED), (f) particle size distribution curve and (g) EDS spectra of rGS-Ag-3 composites.

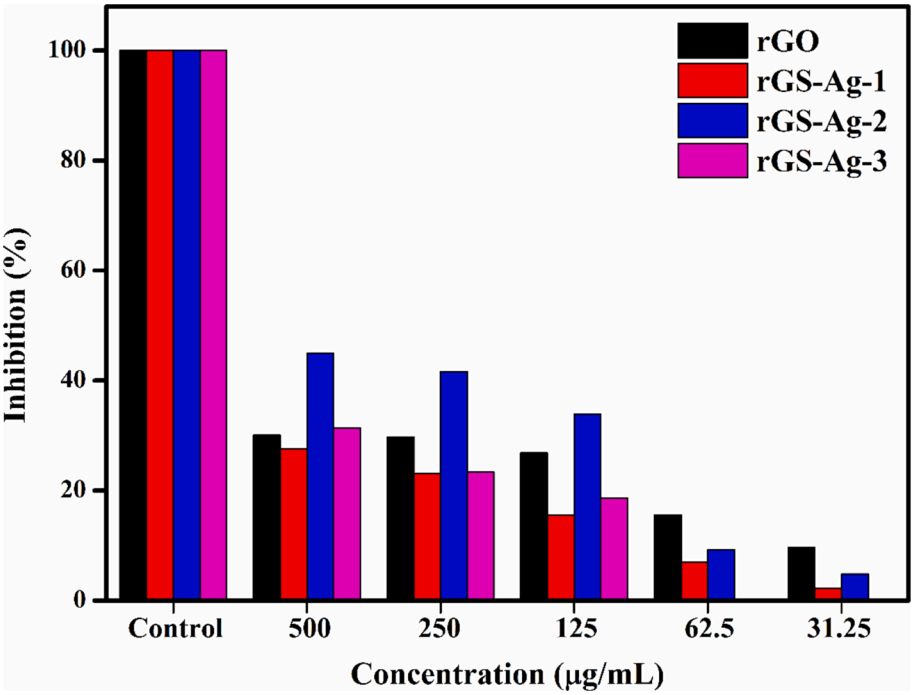

Fig. 4. Correlation graph of Anti Biofilm Activity.

antibio film activity using two different types of peper solution stabilized AgNPs [59]. The degradation of dentine arises due to the interactions prevailing between the substrate surface, bacterial cells, and their metabolic product in the nutrient-deprived medium. rGS-Ag-2 was found to have a higher percentage of inhibition of about 44.99 % in biofilm degradation which is given in Table 1. Furthermore, the values for the maximum anti-biofilm activity of the AgNPs nanoparticles against different pathogens are provided in Table 2, which includes previous experimental results for better comprehension.

3.2. Photocatalytic activity

The photocatalytic efficiency of the prepared catalysts viz., rGO, rGO/SL, rGS-Ag-1 rGS-Ag-2 rGS-Ag-3 composites were examined through photodegradation of methylene blue (MB) by pseudo-first-order reaction condition. The MB degradation under visible light irradiation was monitored by decreasing trends of UV–Visible characteristic peaks at 664 nm. In the blank test, the MB does not degrade under the light absence of photocatalysts, thus results reveal that MB is more stable. Further, mild absorption occurred in photocatalysts without light sources, thus revealing that MB is very stable in the presence of light. The photodegradation of rGO and rGO/SL was found to be an average activity, after 60 min irradiation. After loading of AgNPs onto the surface of rGO/SL, the photodegradation efficiency increased, due to electron charge carrier and high electron-hole pair recombination. All the rGO/SL-Ag composites are excellent photocatalytic activity. Particularly, the rGS-Ag-3 composites are more efficient than rGS-Ag-1 and rGS-Ag-2, the active sites are increased by increasing the AgNPs metal loading.

Table 1
Anti-biofilm activities of prepared rGO, rGS-Ag-1, rGS-Ag-2 and rGS-Ag-3 composites.

S. No.	Tested sample concentration (µg/mL)	Percentage of inhibition			
		rGO	rGS-Ag-1	rGS-Ag-2	rGS-Ag-3
1	Control	100	100	100	100
2	500	30.064	27.61	44.991	31.396
3	250	29.748	23.07	41.615	23.374
4	125	26.843	15.55	33.883	18.642
5	62.5	15.583	7.04	9.196	0
6	31.25	9.679	2.25	4.828	0

Table 2
Comparisons of antibiofilm activity of nanoparticles with previous reports.

Samples	MIC (IC50) µg/ml	Pathogens	References
G. lanceolarium-AgNPs	68.94 ± 0.2	P. aeruginosa, E. coli, and S. aureus	[42]
S. anacardium – AgNPs	12.9 ± 0.2	P. aeruginosa, E. coli, and S. aureus	[42]
B. retusa - AgNPs	23.48 ± 0.2	P. aeruginosa, E. coli, and S. aureus	[42]
HWP/GBP AgNPs	50	S. aureus	[59]
rGS-Ag-1	44.99 ± 0.2	bacteria *Enterococcus faecalis* -MTCC. No. 439	This work

The obtained results showed that the concentration of MB dye solution decreased with increasing the irradiation time. The percentage of degradation efficiency was calculated by the relative intensity of UV–Visible spectra using the below-mentioned equation.

$$\%\ \text{degradation efficiency} = 1 - \frac{C_o}{C_t} X100 \quad (2)$$

Where C_0 is referred to as the initial concentration of MB solution, and C_t means the concentration of MB at various intervals of time. the absorption of MB dye depicts a reducing trend with the rise in exposure time in the light. The rate constants (k) values of the photocatalytic reaction were calculated using the pseudo-first-order kinetics Eq. (2).

$$-\ln\left(\frac{C}{C_o}\right) = kt \quad (3)$$

Let C represent the initial concentration of MB, and C_0 represent the concentration of MB after a particular interval of time (t).

Fig. 5a shows that the photodegradation of (C/C_0) vs time explains the degradation of MB. Further, Fig. 5b shows that the line slope values

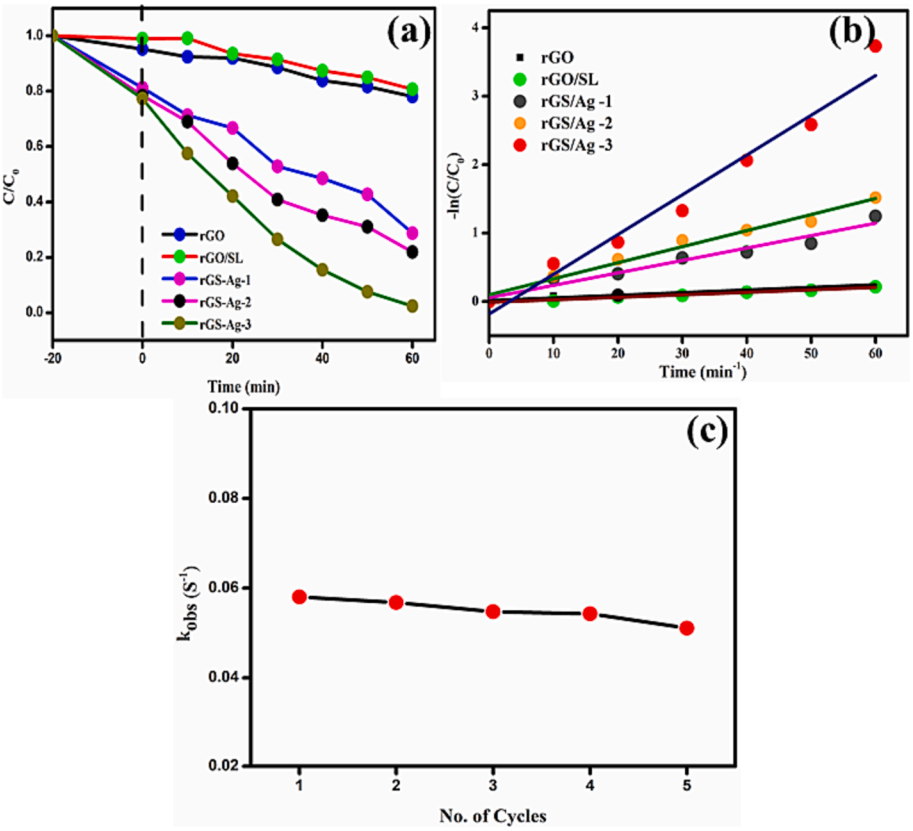

Fig. 5. Photodegradation of MB over rGO, rGO/Sl, rGS-Ag-1, rGS-Ag-2 and rGS-Ag-3.

were used to calculate the rate constants. The maximum rate constants reveal the efficiency of photocatalysts. The rate constant values are given in Table 3. Based on the rate constant values rGO/SL-supported AgNPs show better catalytic activity than pure rGO and rGO/SL. Further, rGS-Ag-3 hows better catalytic performance than rGS-Ag-1 and rGS-Ag-2. It can be also concluded that the in-situ synthesized catalysts remarkably show the separation of photogenerated electron-hole pairs in rGS-Ag NPs for photodegradation. The recycling efficiency of the rGS-Ag-3 composites was examined through the photodegradation of MB using under identical conditions. The catalysts particles were recovered by centrifugal process and reused up to 5th cycle and a graph is drawn from degradation efficiency vs recycling time (Fig. 5c). The obtained results show that the rGS-Ag-3 composites are found to be constant degradation efficiency upto fifth cycle. Thus results reveal that SL and AgNPs are strongly bound on the surface of rGO and there is no metal leaching or aggregation occurring during the recycling time. Furthermore, after five consecutive cycles, the recovered rGS-Ag-3 catalyst composites were washed with a water–ethanol mixture, and the obtained reused catalysts were analyzed by EDS analysis (as shown in Fig. 6). The EDS analysis results illustrate that the rGS-Ag-3 composites contain a reasonable amount of C, N, O, Na, S, and AgNPs. The sample containing 42, 1.30, 36.07, 10.34, 6.30 and 3.46 atomic wt % of C, N, O, Na, S and Ag, respectively. Further, the values of the maximum degradation efficiency of MB are listed in Table 4 where previous experimental results are included for better understanding.

Table 3
Photodegradation efficiency and rate constant of the prepared samples for MB.

Entry	rGO	rGO/SL	rGS-Ag-1	rGS-Ag-2	rGS-Ag-3
$K^{-1}_{obs\ s}$	0.00386	0.00364	0.01816	0.02347	0.05807
R^2	0.9870	0.9919	0.9718	0.9895	0.9792
Degradation efficiency (%) (60 min.)	10.77	19.28	71.27	78.07	96.48

3.3. The photocatalytic mechanism

The 2-D structure of rGO enables a highly efficient transfer of charge carriers, ensuring excellent conductivity. The proposed mechanism envisions Ag nanoparticles as acting like antennae for visible light, while rGO plays a critical role in effectively separating electrons and holes [64]. When exposed to visible light, the RGO/Ag nanocomposites undergo an electron transition from the valence band of silver to the conduction band due to a narrow band gap. The photoelectron successfully surmounts the Schottky barrier between Ag nanoparticles and the graphene sheet, transferring to the graphene sheet itself [65]. This leads to a significant separation of electrons and holes. The subsequent reaction of these electrons with dissolved oxygen creates reactive oxygen species, while holes on Ag interact with water molecules, producing hydroxyl radicals (Fig. 7). Together, they drive the degradation of organic pollutants. Among the synthesized RGO/Ag samples, AgNPs demonstrate the highest photocatalytic activity. However, an excessive addition of rGO may attenuate this activity. An abundance of rGO could hinder the light absorption of Ag nanoparticles, thus impeding electron generation. Furthermore, an excess of GO may cover the active sites on the surface of Ag nanoparticles, consequently reducing photocatalytic activity. This underscores the importance of striking an optimal balance between rGO and Ag nanoparticles to facilitate efficient electron transportation.

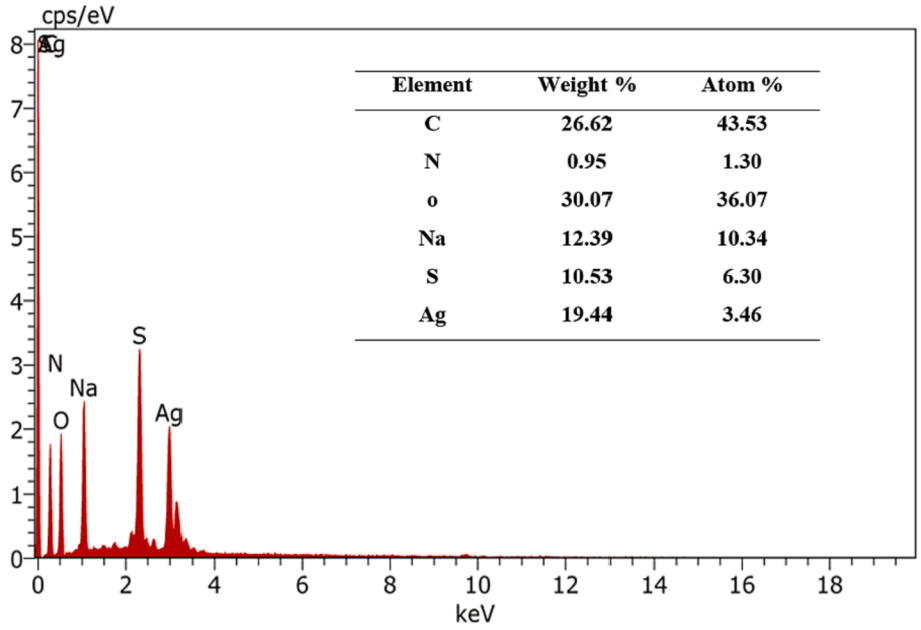

Element	Weight %	Atom %
C	26.62	43.53
N	0.95	1.30
o	30.07	36.07
Na	12.39	10.34
S	10.53	6.30
Ag	19.44	3.46

Fig. 6. EDS spectrum of rGS-Ag-3 after photodegrdadation of MB.

Table 4
Comparisons of photocatalytic performance towards MB with previous reports.

Samples	Quantity of MB(mg/L)	Dosage of photocatalyst(mg)	Photocatalytic duration(min)	Degradation efficiency	References
TiO_2-rGO composite	10	1	300	98.72	[60]
rGO/Ag/Fe doped TiO_2	20	10	150	95.33	[61]
Ag-ZnO/rGO	10	50	120	94.5	[62]
rGO/AgNWs	20	20	90	98.36	[63]
rGS-Ag-1	10	5	60	96.48	This work

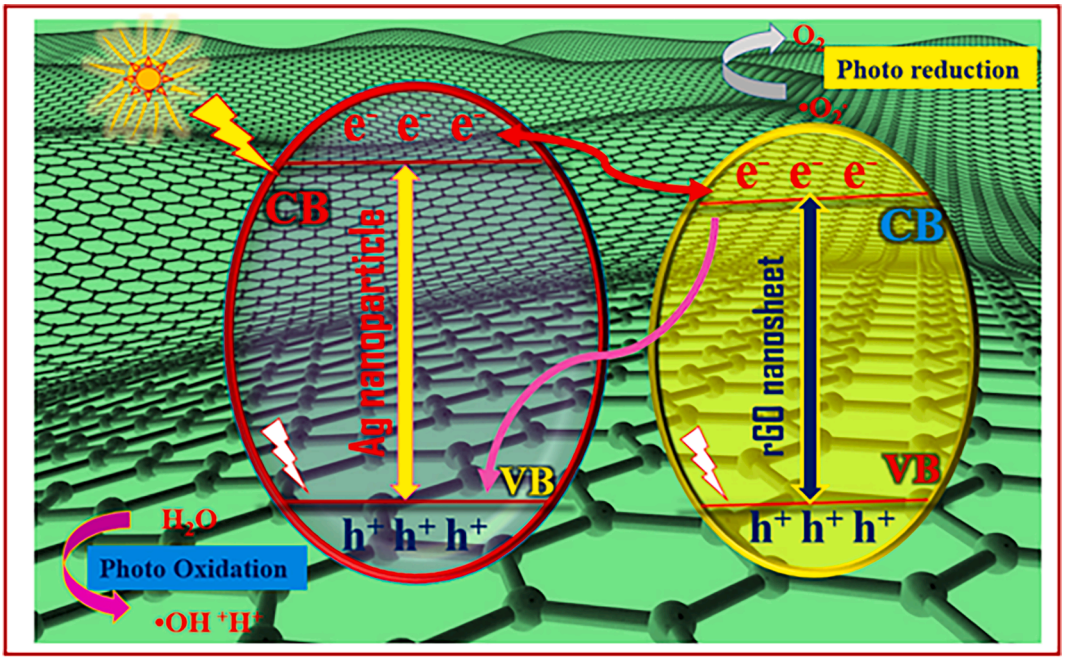

Fig. 7. Proposed mechanism for the Photodegration of MB over ag/rGO composites under visible-light irradiation.

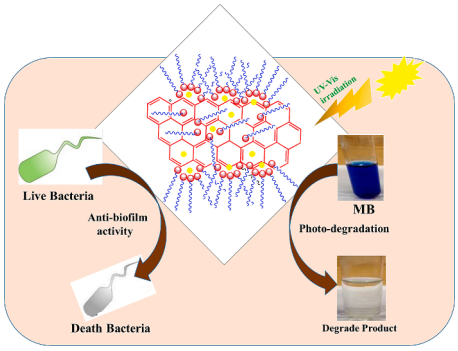

Graphical abstract

4. Conclusions

This work accomplished the multifunctional effects of composites based on non-covalent functionalized rGO/SL with AgNPs. An eco-friendly, facile and simple method was recognized to synthesize nanocomposite. The rGS-AgNPs composites were fabricated using a simple non-covalent functionalization method followed by a chemical reduction process. This non-covalent functionalization method helps prevent structural defects on the surface of the rGO.The crystallinity, surface functional groups, size, shape, surface morphology and elemental composition was thoroughly characterized by different types of spectroscopic and microscopic techniques. The surface loading of surfactant-stabilized AgNPs with rGO nanosheets was confirmed by HRTEM analysis. The size of the rGO/SL supported AgNPs are found to be 8–10 nm, the smaller-sized rGS-AgNP nanosheets examined excellent morphology and exhibit efficient anti-biofilm and photocatalytic activity. The obtained results showed that the rGS-AgNPs composites materials are excellent anti-biofilm activity and photocatalytic activity. Particularly, the rGS-Ag-3 composites showed more outstanding activity than the rest of the composite materials. The rGS-Ag-3 composites achieved 96.48 % of degradation efficiency within 60 min. The composite materials are highly active due to the stabilization of anionic surfactant-stabilized AgNPs and reduced particle size to enhance the active surface. In the future, the experimental studies will be expanded to encompass the non-covalent functionalization various types of surfactants including anionic, catationc and non-ionic coated with graphene oxide supported metal nanocomposies. Furthermore, there will be a focus on evaluating their potential applications in diverse areas. One such area of interest will be the investigation of their biological activities against a wide range of pathogens, which can provide valuable insights into their antimicrobial properties. Additionally, the growth of nanocomposites will be explored as another potential application such as biosensors, food packaging technology, as well as biomedical and pharmaceutically significant reactions. By broadening the scope of the experimental studies, researchers aim to uncover new possibilities and applications for metal oxide nanoparticles, thereby contributing to the advancement of scientific knowledge in this field.

CRediT authorship contribution statement

Usan Pathinathan Saleth Prabhakar: Conceptualization, Investigation. **Paramasivam Shanmugam:** Writing – original draft, Review and editing. **Supakorn Boonyuen:** Methodology, Project administration, Supervision. **Lakshmi Prabha Chandrasekar:** Resources, Software. **Ramyakrishna Pothu:** Writing – review & editing, Formal analysis. **Rajender Boddula:** Conceptualization, Writing – original draft, Writing – review & editing. **Ahmed Bahgat Radwan:** Resources. **Noora Al-Qahtani:** Methodology, Formal analysis, Funding, Supervision.

Declaration of Competing Interest

The authors declare that they have no known competing financial interests or personal relationships that could have appeared to influence the work reported in this paper.

Acknowledgment

The authors gratefully acknowledge the Thammasat University Postdoctoral Fellowship (B.E.2564). This work was supported by Qatar University through a National Capacity Building program Grant (NCBP), [QUCP-CAM-20/23-463]. Statements made herein are solely the responsibility of the authors.

Appendix A. Supplementary data

Supplementary data to this article can be found online at https://doi.org/10.1016/j.mset.2023.10.005.

References

[1] N.T. Loux, Y.S. Su, S.M. Hassan, Issues in assessing environmental exposures to manufactured nanomaterials, Int. J. Environ. Res. Public Health 8 (2011) 3562–3578, https://doi.org/10.3390/ijerph8093562.
[2] L. Thangavelu, G.R. Veeraragavan, S.K. Mallineni, E. Devaraj, R.P. Parameswari, N. H. Syed, K. Dua, D.K. Chellappan, S.R. Balusamy, U.K. Bhawal, Role of nanoparticles in environmental remediation: an insight into heavy metal pollution from dentistry, Bioinorg. Chem. Appl. 2022 (2022) e1946724.
[3] P. Kumar Das, C. Mohanty, G. Krishna Purohit, S. Mishra, S. Palo, Nanoparticle assisted environmental remediation: Applications, toxicological implications and recommendations for a sustainable environment, Environ. Nanotechnol. Monit. Manag. 18 (2022), 100679, https://doi.org/10.1016/j.enmm.2022.100679.
[4] S. Palaniappan, B. Rajender, A novel polyaniline-silver nitrate-p-toluenesulfonic acid salt as recyclable catalyst in the stereoselective synthesis of β-amino ketones: "one-pot" synthesis in water medium, Adv. Synth. Catal. 352 (2010) 2507–2514, https://doi.org/10.1002/adsc.201000346.
[5] P. Shanmugam, R.C. Ngullie, S. Meejoo Smith, S. Boonyuen, R. Boddula, R. Pothu, Visible-light induced photocatalytic removal of methylene blue dye by copper oxide decorated zinc oxide nanorods, Mater. Sci. Energy Technol. 6 (2023) 359–367, https://doi.org/10.1016/j.mset.2023.03.001.
[6] M. Hassanpour, H. Safardoust-Hojaghan, M. Salavati-Niasari, Degradation of methylene blue and Rhodamine B as water pollutants via green synthesized Co3O4/ZnO nanocomposite, J. Mol. Liq. 229 (2017) 293–299, https://doi.org/10.1016/j.molliq.2016.12.090.
[7] B. Parasuraman, B. Kandasamy, I. Murugan, M.S. Alsalhi, N. Asemi, P. Thangavelu, S. Perumal, Designing the heterostructured FeWO4/FeS2 nanocomposites for an enhanced photocatalytic organic dye degradation, Chemosphere 334 (2023), 138979, https://doi.org/10.1016/j.chemosphere.2023.138979.
[8] K. Elghniji, M. Ksibi, E. Elaloui, Sol–gel reverse micelle preparation and characterization of N-doped TiO2: Efficient photocatalytic degradation of methylene blue in water under visible light, J. Ind. Eng. Chem. 18 (2012) 178–182, https://doi.org/10.1016/j.jiec.2011.11.011.
[9] P. Shanmugam, W. Wei, K. Qian, Z. Jiang, J. Lu, J. Xie, Efficient removal of erichrome black T with biomass-derived magnetic carbonaceous aerogel sponge, Mater. Sci. Eng. B 248 (2019), 114387, https://doi.org/10.1016/j.mseb.2019.114387.
[10] P. Shanmugam, K. Rajakumar, R. Boddula, R.C. Ngullie, W. Wei, J. Xie, E. Murugan, Heterogeneous form of poly (4-vinyl pyridine) beads based dendrimer stabilized Ag, Au and PdNPs catalyst for reduction of trypan blue, Mater. Sci. Energy Technol. 2 (2019) 532–542, https://doi.org/10.1016/j.mset.2019.05.006.
[11] M. Saeed, A. Ahmad, R. Boddula, Inamuddin, A. ul Haq, A. Azhar, Ag@MnxOy: an effective catalyst for photo-degradation of rhodamine B dye, Environ. Chem. Lett. 16 (2018) 287–294, https://doi.org/10.1007/s10311-017-0661-z.
[12] B. Parasuraman, V. Vasudevan, B. Kandasamy, H. Rangaraju, P. Thangavelu, Development of Bi2S3/Cu2S hetrojuction as an effective photocatalysts for the efficient degradation of antibiotic drug and organic dye, Environ. Sci. Pollut. Res. (2023), https://doi.org/10.1007/s11356-023-26627-9.
[13] U.P.S. Prabhakar, Synthesis, structural elucidation of metal nanoparticles prepared from metal complexes via thermal decomposition method, Appl. Surf. Sci. Adv. 13 (2023) 100357, https://doi.org/10.1016/j.apsadv.2022.100357.
[14] K.G.U.R. Kumarasinghe, W.C.H. Silva, M.D.A. Fernando, L. Palliyaguru, P. S. Jayawardena, M. Shimomura, S.S.N. Fernando, T.D.C.P. Gunasekara, P. M. Jayaweera, One-pot reducing agent-free synthesis of silver nanoparticles/nitrocellulose composite surface coating with antimicrobial and antibiofilm activities, Biomed Res. Int. 2021 (2021) e6666642.
[15] R.P. Carlson, R. Taffs, W.M. Davison, P.S. Stewart, Anti-biofilm properties of chitosan-coated surfaces, J. Biomater. Sci. Polym. Ed. 19 (2008) 1035–1046, https://doi.org/10.1163/156856208784909372.
[16] A. Varma, A. Warghane, N.K. Dhiman, N. Paserkar, V. Upadhye, A. Modi, R. Saini, The role of nanocomposites against biofilm infections in humans, accessed June 26,

2023, Front. Cell. Infect. Microbiol. 13 (2023), https://www.frontiersin.org/articles/10.3389/fcimb.2023.1104615.
[17] D. Maiti, X. Tong, X. Mou, K. Yang, Carbon-based nanomaterials for biomedical applications: a recent study, accessed May 2, 2023, Front. Pharmacol. 9 (2019), https://www.frontiersin.org/articles/10.3389/fphar.2018.01401.
[18] A.L.T. Zheng, S. Boonyuen, G.Y. Li, L.H. Ngee, Y. Andou, Design of reduced graphene hydrogel with alkylamine surface functionalization through immersion/agitation method and its adsorption mechanism, J. Mol. Struct. 1245 (2021) 131008, https://doi.org/10.1016/j.molstruc.2021.131008.
[19] E. Mostafavi, H. Zare, Carbon-based nanomaterials in gene therapy, OpenNano. 7 (2022), 100062, https://doi.org/10.1016/j.onano.2022.100062.
[20] V. Ramar, A. Balraj, Critical review on carbon-based nanomaterial for carbon capture: technical challenges, opportunities, and future perspectives, Energy Fuels 36 (2022) 13479–13505, https://doi.org/10.1021/acs.energyfuels.2c02585.
[21] R.C. Ngullie, P. Shanmugam, M.H. Mahmoud, U. Pathinathan Saleth Prabhakar, M. L. Aruna Kumari, M. Shaheer Akhtar, Fabrication of biomass derived carbon supported iron oxide composites for antibacterial and antifungal activity, Mater. Lett. 312 (2022), 131664, https://doi.org/10.1016/j.matlet.2022.131664.
[22] P. Shanmugam, S.M. Smith, S. Boonyuen, A. Luengnaruemitchai, In-situ development of boron doped g-C3N4 supported SBA-15 nanocomposites for photocatalytic degradation of tetracycline, Environ. Res. 224 (2023), 115496, https://doi.org/10.1016/j.envres.2023.115496.
[23] M.S. AlSalhi, S. Devanesan, P. Shanmugam, Y.O. Kim, J.-T. Kwon, H.-J. Kim, Synthesis and biocompatible role of hierarchical structured carbon nanoplates incorporated α-Fe2O3 nanocomposites for biomedical applications with respect to cancer treatment, Saudi Journal of Biological Sciences 27 (2020) 588–593, https://doi.org/10.1016/j.sjbs.2019.11.028.
[24] P. Xiong, Y. Fu, L. Wang, X. Wang, Multi-walled carbon nanotubes supported nickel ferrite: A magnetically recyclable photocatalyst with high photocatalytic activity on degradation of phenols, Chem. Eng. J. 195–196 (2012) 149–157, https://doi.org/10.1016/j.cej.2012.05.007.
[25] R. Boddula, R. Bolagam, P. Srinivasan, Incorporation of graphene-Mn3O4 core into polyaniline shell: supercapacitor electrode material, Ionics 24 (2018) 1467–1474, https://doi.org/10.1007/s11581-017-2300-x.
[26] D. González-Muñoz, A. Martín-Somer, K. Strobl, S. Cabrera, P.J. De Pablo, S. Díaz-Tendero, M. Blanco, J. Alemán, Enhancing visible-light photocatalysis via endohedral functionalization of single-walled carbon nanotubes with organic dyes, ACS Appl. Mater. Interfaces 13 (2021) 24877–24886, https://doi.org/10.1021/acsami.1c04679.
[27] H. Ahmad, M. Fan, D. Hui, Graphene oxide incorporated functional materials: A review, Compos. B Eng. 145 (2018) 270–280, https://doi.org/10.1016/j.compositesb.2018.02.006.
[28] A.K.R. Police, M. Chennaiahgari, R. Boddula, S.V.P. Vattikuti, K.K. Mandari, B. Chan, Single-step hydrothermal synthesis of wrinkled graphene wrapped TiO2 nanotubes for photocatalytic hydrogen production and supercapacitor applications, Mater. Res. Bull. 98 (2018) 314–321, https://doi.org/10.1016/j.materresbull.2017.10.034.
[29] Q. Zhou, D. Li, T. Wang, X. Hu, Leaching of graphene oxide nanosheets in simulated soil and their influences on microbial communities, J. Hazard. Mater. 404 (2021), 124046, https://doi.org/10.1016/j.jhazmat.2020.124046.
[30] V. Georgakilas, M. Otyepka, A.B. Bourlinos, V. Chandra, N. Kim, K.C. Kemp, P. Hobza, R. Zboril, K.S. Kim, Functionalization of graphene: covalent and non-covalent approaches, derivatives and applications, Chem. Rev. 112 (2012) 6156–6214, https://doi.org/10.1021/cr3000412.
[31] S.R. Eedulakanti, A.K. Gampala, K. Venkateswara Rao, C.h. Shilpa Chakra, V. Gedela, R. Boddula, Ultrasonication assisted thermal exfoliation of graphene-tin oxide nanocomposite material for supercapacitor, Mater. Sci. Energy Technol. 2 (2019) 372–376, https://doi.org/10.1016/j.mset.2019.03.007.
[32] K. Viswanathan, T. Ravi, R. Boddula, Synthesis graphene based sensor for strain data and its characterization, Mater. Sci. Energy Technol. 2 (2019) 203–207, https://doi.org/10.1016/j.mset.2019.01.003.
[33] S. Stankovich, D.A. Dikin, R.D. Piner, K.A. Kohlhaas, A. Kleinhammes, Y. Jia, Y. Wu, S.T. Nguyen, R.S. Ruoff, Synthesis of graphene-based nanosheets via chemical reduction of exfoliated graphite oxide, Carbon 45 (2007) 1558–1565, https://doi.org/10.1016/j.carbon.2007.02.034.
[34] R. Ikram, B.M. Jan, W. Ahmad, An overview of industrial scalable production of graphene oxide and analytical approaches for synthesis and characterization, J. Mater. Res. Technol. 9 (2020) 11587–11610, https://doi.org/10.1016/j.jmrt.2020.08.050.
[35] Mechanism of Graphene Oxide Formation | ACS Nano, (n.d.). https://pubs.acs.org/doi/10.1021/nn500606a (accessed June 21, 2023).
[36] N. Saha, E. Fillerup, B. Thomas, C. Pilgrim, T. Causer, D. Herren, J. Klinger, Improving bamboo's fuel and storage properties with a net energy export through torrefaction paired with catalytic oxidation, Chem. Eng. J. 440 (2022), 135750, https://doi.org/10.1016/j.cej.2022.135750.
[37] R. Bolagam, R. Boddula, P. Srinivasan, Design and synthesis of ternary composite of polyaniline-sulfonated graphene oxide-TiO2 nanorods: a highly stable electrode material for supercapacitor, J. Solid State Electrochem. 22 (2018) 129–139, https://doi.org/10.1007/s10008-017-3732-y.
[38] J. Ma, J. Liu, W. Zhu, W. Qin, Solubility study on the surfactants functionalized reduced graphene oxide, Colloids Surf. Physicochem. Eng. Asp. 538 (2018) 79–85, https://doi.org/10.1016/j.colsurfa.2017.10.071.
[39] C. Bosch-Navarro, Z.P.L. Laker, A.J. Marsden, N.R. Wilson, J.P. Rourke, Non-covalent functionalization of graphene with a hydrophilic self-limiting monolayer for macro-molecule immobilization, FlatChem. 1 (2017) 52–56, https://doi.org/10.1016/j.flatc.2016.11.001.
[40] V. Georgakilas, J.N. Tiwari, K.C. Kemp, J.A. Perman, A.B. Bourlinos, K.S. Kim, R. Zboril, Noncovalent functionalization of graphene and graphene oxide for energy materials, biosensing, catalytic, and biomedical applications, Chem. Rev. 116 (2016) 5464–5519, https://doi.org/10.1021/acs.chemrev.5b00620.
[41] S. ul Haque, Inamuddin, A. Nasar, B. Rajender, A. Khan, A.M. Asiri, G.M. Ashraf, Optimization of glucose powered biofuel cell anode developed by polyaniline-silver as electron transfer enhancer and ferritin as biocompatible redox mediator, Sci. Rep. 7 (2017) 12703, https://doi.org/10.1038/s41598-017-12708-6.
[42] Y.K. Mohanta, K. Biswas, S.K. Jena, A. Hashem, E.F. Abd_Allah, T.K. Mohanta, Anti-biofilm and antibacterial activities of silver nanoparticles synthesized by the reducing activity of phytoconstituents present in the indian medicinal plants, accessed May 2, 2023, Front. Microbiol. 11 (2020), https://www.frontiersin.org/articles/10.3389/fmicb.2020.01143.
[43] X. Chen, J. Lei, Y. Wang, W. Zhu, W. Yao, T. Duan, Ternary Ag nanoparticles/natural-magnetic SiO2-nanowires/reduced graphene oxide nanocomposites with highly visible photocatalytic activity for 4-nitrophenol reduction, SN Appl. Sci. 1 (2018) 130, https://doi.org/10.1007/s42452-018-0124-6.
[44] P. Wang, D. Wu, Y. Ao, C. Wang, J. Hou, ZnO nanorod arrays co-loaded with Au nanoparticles and reduced graphene oxide: Synthesis, characterization and photocatalytic application, Colloids Surf. Physicochem. Eng. Asp. 492 (2016) 71–78, https://doi.org/10.1016/j.colsurfa.2015.12.006.
[45] J. Song, X. Wang, C.-T. Chang, Preparation and characterization of graphene oxide, J. Nanomater. 2014 (2014) e276143.
[46] C. Wang, J. Zhou, J. Ni, Y. Cheng, H. Li, Design and synthesis of pyrophosphate acid/graphene composites with wide stacked pores for methylene blue removal, Chem. Eng. J. 253 (2014) 130–137, https://doi.org/10.1016/j.cej.2014.05.020.
[47] X. Huang, J. Zhang, W. Rao, T. Sang, B. Song, C. Wong, Tunable electromagnetic properties and enhanced microwave absorption ability of flaky graphite/cobalt zinc ferrite composites, J. Alloy. Compd. 662 (2016) 409–414, https://doi.org/10.1016/j.jallcom.2015.12.076.
[48] S.A. Soomro, I.H. Gul, H. Naseer, S. Marwat, M. Mujahid, Improved Performance of CuFe2O4/rGO Nanohybrid as an Anode Material for Lithium-ion Batteries Prepared Via Facile One-step Method, Curr. Nanosci. 15 (n.d.) 420–429. https://www.eurekaselect.com/article/94573 (accessed May 3, 2023).
[49] H. Chang, G. Wang, A. Yang, X. Tao, X. Liu, Y. Shen, Z. Zheng, A. Transparent, Flexible, low-temperature, and solution-processible graphene composite electrode, Adv. Funct. Mater. 20 (2010) 2893–2902, https://doi.org/10.1002/adfm.201000900.
[50] S. Sang, D. Li, H. Zhang, Y. Sun, A. Jian, Q. Zhang, W. Zhang, Facile synthesis of AgNPs on reduced graphene oxide for highly sensitive simultaneous detection of heavy metal ions, RSC Adv. 7 (2017) 21618–21624, https://doi.org/10.1039/C7RA02267K.
[51] E. Murugan, S. Santhosh Kumar, K.M. Reshna, S. Govindaraju, Highly sensitive, stable g-CN decorated with AgNPs for SERS sensing of toluidine blue and catalytic reduction of crystal violet, J. Mater. Sci. 54 (2019) 5294–5310, https://doi.org/10.1007/s10853-018-3184-5.
[52] I.O. Faniyi, O. Fasakin, B. Olofinjana, A.S. Adekunle, T.V. Oluwasusi, M.A. Eleruja, E.O.B. Ajayi, The comparative analyses of reduced graphene oxide (RGO) prepared via green, mild and chemical approaches, SN Appl. Sci. 1 (2019) 1181, https://doi.org/10.1007/s42452-019-1188-7.
[53] E. Murugan, G. Vimala, Synthesis, characterization, and catalytic activity for hybrids of multi-walled carbon nanotube and amphiphilic poly(propyleneimine) dendrimer immobilized with silver and palladium nanoparticle, J. Colloid Interface Sci. 396 (2013) 101–111, https://doi.org/10.1016/j.jcis.2012.12.074.
[54] J.P. Mensing, A. Wisitsoraat, D. Phokharatkul, T. Lomas, A. Tuantranont, Novel surfactant-stabilized graphene-polyaniline composite nanofiber for supercapacitor applications, Compos. B Eng. 77 (2015) 93–99, https://doi.org/10.1016/j.compositesb.2015.03.004.
[55] J. Yang, J. Sun, Z. Wang, L. Wang, Surfactant-modified graphene oxide complex-coating functionalized material with robust switchable oil/water wettability for high-performance on-demand emulsion separation, Surf. Coat. Technol. 439 (2022), 128431, https://doi.org/10.1016/j.surfcoat.2022.128431.
[56] B. Abreu, A.S. Pires, A. Guimarães, R.M.F. Fernandes, I.S. Oliveira, E.F. Marques, Polymer/surfactant mixtures as dispersants and non-covalent functionalization agents of multiwalled carbon nanotubes: Synergism, morphological characterization and molecular picture, J. Mol. Liq. 347 (2022), 118338, https://doi.org/10.1016/j.molliq.2021.118338.
[57] C. Cheng, W.-H. Shi, T.-P. Teng, C.-R. Yang, Evaluation of surfactants on graphene dispersion and thermal performance for heat dissipation coating, Polymers 14 (2022) 952, https://doi.org/10.3390/polym14050952.
[58] A. Kisielewska, K. Spilarewicz-Stanek, M. Cichomski, W. Kozłowski, I. Piwoński, The role of graphene oxide and its reduced form in the in situ photocatalytic growth of silver nanoparticles on graphene-TiO2 nanocomposites, Appl. Surf. Sci. 576 (2022), 151759, https://doi.org/10.1016/j.apsusc.2021.151759.
[59] R. Lotha, B.R. Shamprasad, N.S. Sundaramoorthy, R. Ganapathy, S. Nagarajan, A. Sivasubramanian, Zero valent silver nanoparticles capped with capsaicinoids containing Capsicum annuum extract, exert potent anti-biofilm effect on food borne pathogen Staphylococcus aureus and curtail planktonic growth on a zebrafish infection model, Microb. Pathog. 124 (2018) 291–300, https://doi.org/10.1016/j.micpath.2018.08.053.
[60] S. Umrao, S. Abraham, F. Theil, S. Pandey, V. Ciobota, P.K. Shukla, C.J. Rupp, S. Chakraborty, R. Ahuja, J. Popp, B. Dietzek, A. Srivastava, A possible mechanism for the emergence of an additional band gap due to a Ti–O–C bond in the TiO2–graphene hybrid system for enhanced photodegradation of methylene blue under visible light, RSC Adv. 4 (2014) 59890–59901, https://doi.org/10.1039/C4RA10572A.

[61] D. Prabu Jaihindh, C.-C. Chen, Y.-P. Fu, Reduced graphene oxide-supported Ag-loaded Fe-doped TiO 2 for the degradation mechanism of methylene blue and its electrochemical properties, RSC Adv. 8 (2018) 6488–6501, https://doi.org/10.1039/C7RA13418E.

[62] X. Yu, Z. Li, K. Dang, Z. Zhang, L. Gao, L. Duan, Z. Jiang, J. Fan, P. Zhao, Enhanced photocatalytic activity of Ag–ZnO/RGO nanocomposites for removal of methylene blue, J. Mater. Sci. Mater. Electron. 29 (2018) 8729–8737, https://doi.org/10.1007/s10854-018-8889-3.

[63] J. Singh, A.S. Dhaliwal, Electrochemical and photocatalytic degradation of methylene blue by using rGO/AgNWs nanocomposite synthesized by electroplating on stainless steel, J. Phys. Chem. Solid 160 (2022), 110358, https://doi.org/10.1016/j.jpcs.2021.110358.

[64] I.V. Lightcap, T.H. Kosel, P.V. Kamat, Anchoring semiconductor and metal nanoparticles on a two-dimensional catalyst mat. Storing and shuttling electrons with reduced graphene oxide, Nano Lett. 10 (2010) 577–583, https://doi.org/10.1021/nl9035109.

[65] Z. Mou, Y. Wu, J. Sun, P. Yang, Y. Du, C. Lu, TiO2 nanoparticles-functionalized N-doped graphene with superior interfacial contact and enhanced charge separation for photocatalytic hydrogen generation, ACS Appl. Mater. Interfaces 6 (2014) 13798–13806, https://doi.org/10.1021/am503244w.